20th Australasian Fluid Mechanics Conference
Perth, Australia
5-8 December 2016

# Effect of Wall Confinement on a Wind Turbine Wake

**N. Sedaghatizadeh, M. Arjomandi, R. Kelso, B. Cazzolato, M. H. Ghayesh**

School of Mechanical Engineering
University of Adelaide, Adelaide, South Australia 5005, Australia

## Abstract

This study investigates the effect of wall confinement on a wind turbine wake as a means to guide future wind-tunnel-based wake studies. Large Eddy Simulation was utilised to simulate the wake region for two cases. The first case simulated the NREL phase VI wind turbine in a wind tunnel with 9% blockage. The reason behind selecting this case is the availability of the experimental data in the literature which enabled us in validating the model. The second case was the same turbine located in an unconfined environment, with the same flow upstream velocity. The results show that the wind tunnel walls significantly affect the wake development and its stability, even with a blockage of less than 10%. Tip vortices in the unconfined environment start to break down closer to the turbine compared to the wall-bounded case, resulting in a shorter wake recovery length for the unconfined flow. Vorticity contours reveal coherent vortical structures in the confined wake up to 20 turbine diameters downstream, while these structures dissipate after 16 diameters in an unconfined environment. The calculated power also showed that the turbine in the wind tunnel generates 5.5% more power than that in the unconfined flow. Collectively, these results provide an insight into the effect of walls on the turbine wake in both numerical and experimental studies, offering guidance on how wind tunnel studies relate to real, unconfined flows.

## Introduction

Most experimental studies on wind turbine wakes have been conducted in wind tunnels under controlled conditions to avoid the difficulties associated with experiments conducted in actual wind farms [1]. One of the concerns in wind turbine experiments, especially those with full-sized turbines, is the effect of walls and blockage ratio. Excessive blockage in a closed-section wind tunnel results in accelerated flow around the turbine and changes in the wake development compared to the open field case.

Two approaches are generally used to minimise the effects of wall confinement on the results of wind tunnel experiments. The first is to apply correction factors on some aerodynamic parameters, and the second is to keep the blockage ratio small enough to avoid the wall interactions. In wind turbine wake studies, where the structure and development of the wake is important, the second approach should be used. McTavish et al. [2] stated that the wind turbine wake is not affected by the walls when the blockage ratio is less than 10%. However, the blockage effect in wind turbine wake studies is a function of several parameters such as the blockage ratio (based on rotor swept area), tip speed ratio, number of blades, pitch angle and even the shape of the blades.

In this study, the wake development of the NREL phase VI wind turbine is investigated numerically to test the validity of the 10% limit for blockage ratio by comparing its wake development in a wind tunnel with the development in an unconfined environment.

## Problem Description and Computational Mesh

The NREL phase VI, a two-bladed stall-regulated wind turbine with a rotor diameter of 10.058 m, was selected due to availability of the experimental data in the literature for validation of the numerical model developed in this paper. The NREL experiment was carried out in a large open-loop wind tunnel with a 24.4 m x 36.6 m cross section area [3]. Figure 1 shows the experimental arrangement which was replicated in the computational model. The hub and nacelle in the computational model are simplified in order to reduce the complexity of the model which makes high quality grid generation difficult.

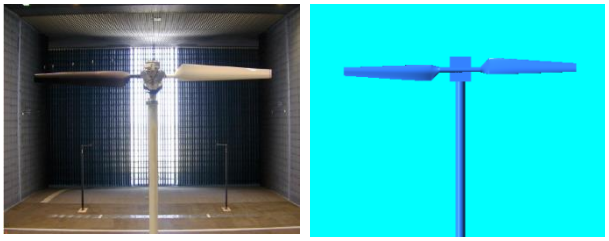

Figure 1 Wind turbine in wind tunnel (left) [3] and computational model (right).

Two computational domains were created, one for the wind tunnel and one for an unconfined environment. The computational domain for the wind tunnel is 24.4m high and 36.6m wide to replicate the experimental wind tunnel. The length of the tunnel is 221.3 m which is equals to twenty-two rotor diameters (see Figure 2). The turbine is placed at a position two diameters downstream from the inlet, in the middle of the wind tunnel. The blockage ratio is 9%.

For the unconfined environment with a uniform wind velocity profile, a larger domain was considered with the wind tunnel computational domain placed in the middle of the computational space. A $y^+ \leq 1$ was used to accurately resolve the boundary layer on the blade surface which resulted approximately 11 and 12.5 million hexahedral cells for wind tunnel and unconfined environment respectively. The computational domains for wind tunnel and unconfined environment are shown in Figure 2.

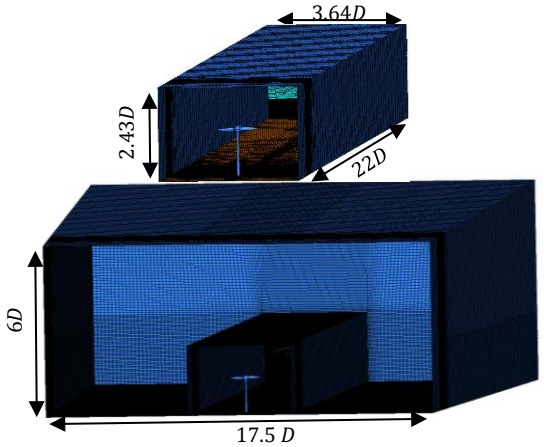


Figure 2 Computational domain for wind tunnel (top) and unconfined environment (bottom). *D* is the diameter of the rotor.

Figure 3 shows the schematic layouts of the cases which were studied.

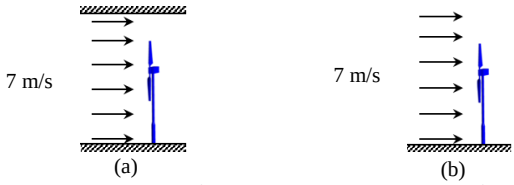

Figure 3 Schematic layout of the two test cases and wind profiles; a) wind tunnel, b) unconfined environment.

Computations were carried out for uniform wind velocity profiles of 7 m/s resulting in Reynolds number of approximately 5 million based on rotor diameter. The blades rotate at a constant speed of 71.9 rpm in both cases. The time step was set to 0.002318 seconds corresponding to a 1 degree rotation of the blade per time-step. LES calculations were carried out using FLUENT 16.2 which is a general-purpose CFD code. Simulations were performed for a sufficiently long period of time (30 revolutions), to ensure the wake was fully developed and the results are statistically stable. After ensuring that the wake was sufficiently developed, results were recorded over 10 revolutions of the wind turbine to calculate the time-average parameters.

## Numerical Method

Large Eddy Simulation (LES) was used to computationally calculate the flow field in the wake of wind turbine. The basic governing equations are the Navier-Stokes, energy and continuity equations which are solved together with appropriate boundary conditions to provide the flow field for the computational domain. In this study, heat transfer and temperature gradients within the fluid domain are negligible, and the focus is on fluid motion, so the energy equation is not considered. Conservation equations are presented below as:

$$\frac{\partial \rho}{\partial t} + \frac{\partial}{\partial x_i}(\rho u_i) = 0 \tag{1}$$

$$\frac{\partial (\rho u_i)}{\partial t} + \frac{\partial (\rho u_j u_i)}{\partial x_j} = \frac{\partial \sigma_{ij}}{\partial x_j} - \frac{\partial p}{\partial x_i} + f_i \tag{2}$$

Here $u$ is the velocity, σ is the stress tensor defined as $\sigma_{ij} = \mu\left(\frac{\partial u_i}{\partial x_j} + \frac{\partial u_j}{\partial x_i}\right) - \frac{2}{3}\mu\frac{\partial u_l}{\partial x_l}\delta_{ij}$, $p$ is the pressure and $f$ represents the body forces.

The governing equations of LES are obtained by filtering the original continuum and Navier-Stokes equations as:

$$\frac{\partial \rho}{\partial t} + \frac{\partial}{\partial x_i}(\rho \overline{u_i}) = 0 \tag{3}$$

$$\frac{\partial (\rho \overline{u_i})}{\partial t} + \frac{\partial (\rho \overline{u_j}\ \overline{u_i})}{\partial x_j} = \frac{\partial \sigma_{ij}}{\partial x_j} - \frac{\partial \bar{p}}{\partial x_i} + \frac{\partial \tau_{ij}}{\partial x_j} \tag{4}$$

In the above equations, $\overline{u}$ is the resolved velocity, σ is the stress tensor due to molecular viscosity, obtained from resolved velocity, and $\tau_{ij}$ is the subgrid scale stress defined as $\tau_{ij} = \rho\overline{u_i u_j} - \rho\overline{u_i}\,\overline{u_j}$. To close the set of equations, the Boussinsque hypothesis is used for calculations as:

$$\tau_{ij} - \frac{1}{3}\tau_{kk}\delta_{ij} = -2\mu_t \overline{S_{ij}} \tag{5}$$

where $\mu_t$ is subgrid turbulent viscosity, calculated using Smagorinsky-Lilly model as $\mu_t = \rho L_s^2 \left|\overline{S}\right|$. Here $\overline{S}$ is the resolved strain rate and $L_s$ is the mixing length for subgrid length scale computed by:

$$\overline{S_{ij}} = \frac{1}{2}\left(\frac{\partial \overline{u_i}}{\partial x_j} + \frac{\partial \overline{u_j}}{\partial x_i}\right) \tag{6}$$

$$|\bar{S}| \equiv \sqrt{2\overline{S_{ij}}\ \overline{S_{ij}}} \tag{7}$$

$$L_s = min\left(\kappa d, C_s V^{1/2}\right) \tag{8}$$

In the above equations, $\kappa$ is the von Karman factor, $d$ is the closest distance to the walls, $C_s$ is the Smagorinsky factor, and $V$ is the volume of the computational cell. The value of the $C_s$ has a significant effect on large-scale fluctuations in mean shear and transitional regimes. In order to address this problem, Germano et al. [4] and following them Lilly [5] proposed a method in which the Smagorinsky constant is calculated dynamically using the resolved motion data [4, 5]. In this study, the dynamic Smagorinsky-Lilly model is applied in order to eliminate limitations imposed by the traditional Smagorinsky-Lilly subgrid-scale model.

## Validation of the Model

To validate the model, the computed pressure distribution on the blade was compared with experimental data from the wind tunnel experiment [3]. The pressure distribution on the blade is caused by angular and axial momentum changes which characterises the wake. Thus, accurate prediction of the pressure coefficient provides information which is required to validate the model. Figure 4 shows a comparison between numerical simulations and experimental results for wind tunnel case. The results show that the developed LES model is a good match with experimental data, having a maximum difference of 8% between the experimental and computational data. It should also be noted that there was a limited number of pressure taps located on the surface of the physical blades and their uncertainty in accurately measuring the surface pressure, especially near the trailing and leading edges, should be taken into account. Higher discrepancies near the tip of the blade could be due to the effect of tip vortices and higher centrifugal forces which creates radial flow towards the tip.

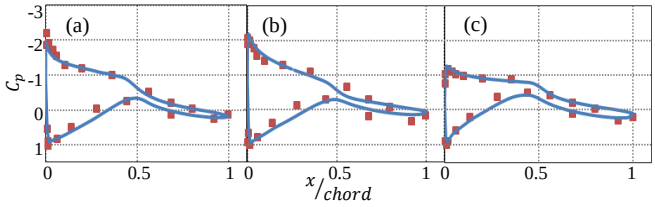

Figure 4 Comparison of the results of the computed pressure coefficient with experiment [3], a) $\frac{r}{R} = 0.3$, b) $\frac{r}{R} = 0.63$, c) $\frac{r}{R} = 0.95$.

Another parameter which can be used to validate the model is the total output power of the blades. Figure 5 shows the fluctuating output power calculated using the computed torque of the blade. The averaged value of the output power obtained from the simulation is 5.73 (kW) which results in 4.6% discrepancy compared with the experimental data [3].

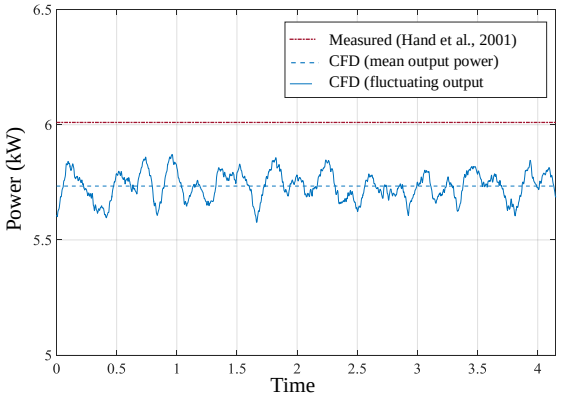

Figure 5 Fluctuating output power for wind tunnel case.

## Results and Discussion

Figure 6 shows the vertical profiles of the normalised axial velocities averaged over time for several normalised locations downstream of the turbine. The effect of the tower is evident for

both cases up to 4*D* downstream. This effect vanishes due to wake growth and turbulent mixing. For both cases the wake is almost axisymmetric about the axis of symmetry located close to the blade axis of rotation, especially for the region corresponding to the rotor blade. This observation is in agreement with previously published data and studies [6]. Passing through the wind turbine, airflow clearly loses its momentum, showing that the turbine is extracting energy from the incoming flow and hence producing a wake. This can be observed from the regions of reduced velocity, or velocity deficit, at *y*/*D*=1 where the W-shaped velocity profiles are apparent. Velocity profiles show that the maximum decay occurs around the blade tip location, which corresponds to the helical ring of tip vortices. Moreover, the wake is spatially constrained by the walls in the wind tunnel, which results in an acceleration in the flow around the outside of the turbine. The velocity profiles also show that the difference between the velocity outside the wake for two cases increases with downstream distance. The velocity increase in the wind tunnel case is caused by both the wake growth and the confinement of the tunnel walls.

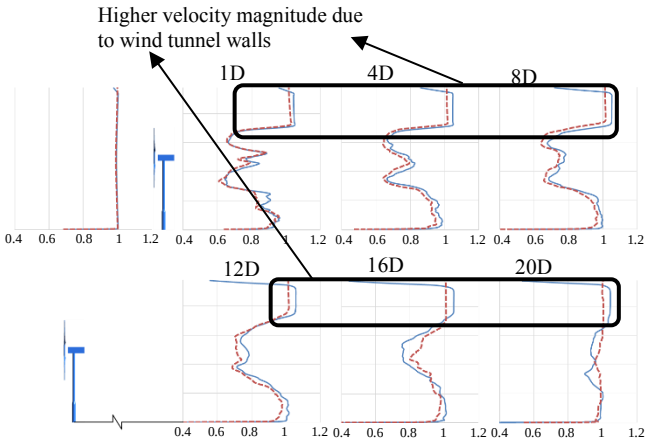


Figure 6 Normalised axial velocity profile downstream of wind turbines (dashed line represents the unconfined environment; solid line represents wind tunnel case).

Time-averaged axial velocity contours for the wind tunnel and unconfined environment are compared in Figure 7. The contours show significant differences in terms of velocity magnitude, wake growth and also wake length between the two cases. Additionally, the effects of the tower shadow can be observed in the region with relatively-reduced velocities in the wake of the tower. In the wind tunnel case this effect dominates closer to the wind turbine by the higher velocity magnitude around the wake area. Whereas the effects of the wake exist for up to 20*D* downstream of the turbine in the wind tunnel simulation, in the unconfined case it vanishes by about 16*D* downstream.

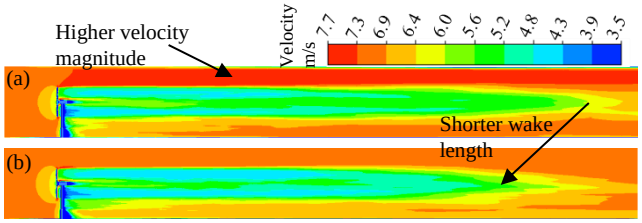


Figure 7 Axial velocity contour on midsection plane in, a) Wind tunnel, b) Unconfined environment.

The fluctuating output power for both cases is shown in Figure 8. The average output power extracted from the blades is higher when turbine is placed in the tunnel. This is due to the blockage effect which increases the velocity deficit, as can be seen in velocity contours (Figure 7). The higher axial-momentum gradient results in higher extracted power in wind tunnel case. Another indicator of the rotor performance is the thrust coefficient. The momentum loss through the rotor plane is balanced by thrust force which is manifested through pressure drop across the rotor. Thrust coefficient can be calculated as $C_T = \frac{\int (P_1 - P_2)\, dA}{\frac{1}{2}\rho A V^2}$, where $P_1$, $P_2$, $A$, and $V$ are pressure in front of the rotor, pressure behind the rotor, area of the rotor, and velocity of the free stream respectively. The experimental thrust coefficient for the wind turbine at a wind speed of 7 m/s was found to be 0.487. The calculated thrust coefficients are 0.4945 and 0.4757 for wind tunnel and unconfined environment cases, respectively. The higher thrust in the wind tunnel can be explained by the flow acceleration due to confinement effect which results in higher pressure drop through the rotor. Thrust coefficient can also be used as a validating parameter which shows only 1.5% deviation from the experimental data.

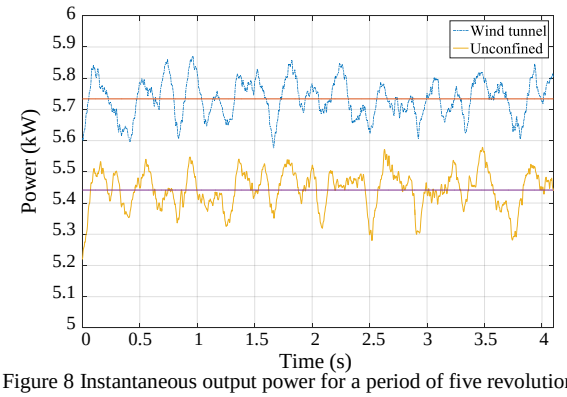


Figure 8 Instantaneous output power for a period of five revolutions of the blades.

The fast Fourier transform (FFT) of the fluctuating power is shown in Figure 9. The FFT was computed for the de-trended fluctuations for 1800 samples over 5 revolutions of the blades. The frequency of the first peak for both cases is equal to blade pass frequency, showing that the fluctuations are related to loads when the blade passes the region affected by the tower. The amplitude of the oscillation is 7.5% larger when the turbine is placed in unconfined environment, which shows that the blades are experiencing higher fatigue loads when there is no closed section around the turbine. It can be concluded that higher momentum and increased velocity due to confinement suppresses the effect of the tower when the turbine is located in the wind tunnel.

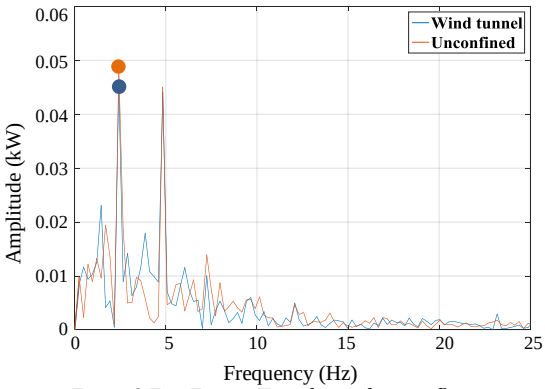


Figure 9 Fast Fourier Transform of power fluctuations.

Vorticity contours in Figure 10 show strong helical rings of tip vortices immediately downstream of the turbine. The ring of vortices is visible up to 4*D* downstream for wind tunnel case. Further downstream the ring starts to break down, and after 6*D* there is no distinct ring of vortices visible. A similar trend is observed for the unconfined environment, with the ring structure being visible up to 7*D* for this case, suggesting that the structure is more stable in the unconfined flow. This difference can be

explained by the higher velocity gradient due to flow acceleration in wind tunnel case. In contrast, by 12*D* downstream the mixing rate in the unconfined environment exceeds the wind tunnel case. From this point the vortical structures become unstable, and without wall confinement, the wake expands faster and the rate of turbulent mixing increases. At 20*D* from the rotor the flow structure has substantially dissipated more in the unconfined flow case.

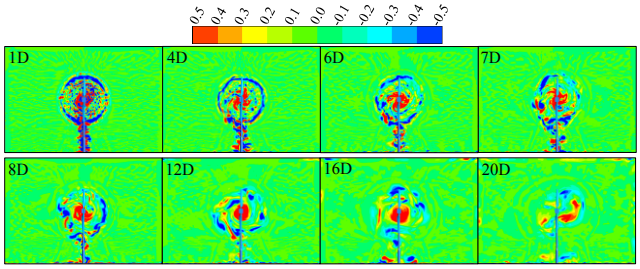


(a) Wind tunnel

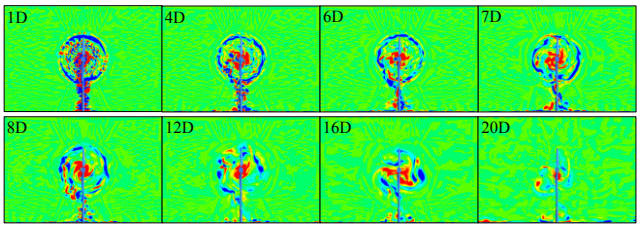


(b) Unconfined environment

Figure 10 Vorticity contours at several locations downstream of turbine.

Figure 11 shows the vorticity contour on the horizontal and vertical midsections. Tip vortices are distinctly visible up to 1.5*D* downstream. However, the trail of tip vortices can be traced far downstream almost up to 20*D* in the wind tunnel and 16*D* in the unconfined flow.

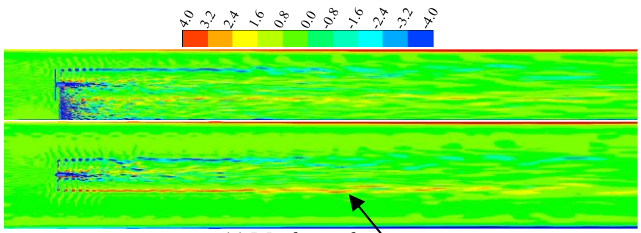


(a) Wind tunnel

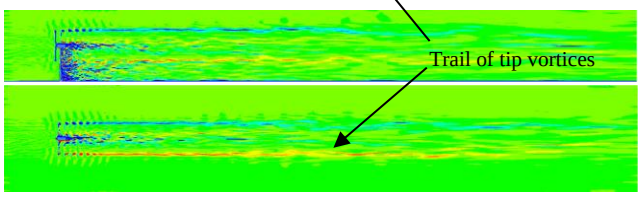


(b) Unconfined environment

Figure 11 Vorticity contour showing the tip vortices downstream of the rotor.

The wake expansion is depicted in Figure 12 using the locations of the tip vortices to define the shear layer width. The wake expansion rate for the unconfined case is slightly higher than that of the wind tunnel case. These effects are attributed directly to the effects of confinement.

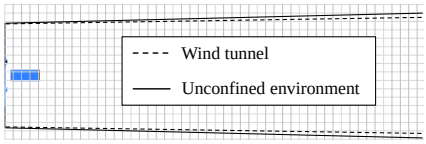


Figure 12 Comparison of wake expansion based on the locations of the tip vortices.

## Conclusion

Large Eddy Simulation was used to investigate the effect of confinement on the wake of an NREL phase VI wind turbine.

Simulation results revealed that confinement has a significant effect on the spatial distribution of the mean velocity profile, wake structure and its development, even when the blockage ratio is less than 10%. The uniform incoming flow in the unconfined environment led to a relatively smaller length of the wake region. The results showed that the wake effect extends up to 20*D* downstream in wind tunnel case and up to 16*D* in unconfined case. Comparing wake expansion based on the location of the tip vortices showed that the unconfined environment has a higher expansion rate compared to wind tunnel case.

A W-shaped velocity profile was observed for all cases immediately behind the wind turbine, with the maximum velocity decay at a tip distance from the axis of rotation. It was observed that removing the surrounding walls results in slightly lower velocity in the wake region up to 12*D* downstream of the wind turbine. Further downstream the wake velocity recovers after 16*D* in unconfined case while region with reduced velocity extends to 20*D* for the wind tunnel.

This study reveals that the 10% limit for blockage ratio reported in previously-published literature is not sufficient to eliminate the effect of wind tunnel walls. Further studies should be carried out in order to specify the effective parameters and their role on blockage effect.

## References


[1] Vermeer, L.J., Sørensen, J.N. & Crespo, A., Wind Turbine Wake Aerodynamics, *Progress in Aerospace Sciences*, **39**, 2003, 467-510.

[2] McTavish, S., Feszty, D. & Nitzsche, F., An Experimental and Computational Assessment of Blockage Effects on Wind Turbine Wake Development, *Wind Energy*, **17**, 2013, 1515-1529.

[3] Hand, M.M., Simms, D.A., Fingersh, L.J., Jager, D.W., Cotrell, J.R., Schreck, S. & Larwood, S.M., *Unsteady Aerodynamics Experiment Phase VI: Wind Tunnel Test Configurations and Available Data Campaigns*, National Renewable Energy Laboratory, U.S Department of Energy Laboratory, 2001.

[4] Germano, M., Piomelli, U., Moin, P. & Cabot, W.H., A Dynamic Subgrid-Scale Eddy Viscosity Model, *Physics of Fluids A*, **3**, 1991, 1760-1765.

[5] Lilly, D.K., A Proposed Modification of the Germano Subgrid-Scale Closure Method, Physics of Fluids A, **4**, 1992, 633-635.

[6] Mo, J.O., Choudhry, A., Arjomandi, M., Kelso, R. & Lee, Y.H., Effects of Wind Speed Changes on Wake Instability of a Wind Turbine in a Virtual Wind Tunnel Using Large Eddy Simulation, *Journal of Wind Engineering and Industrial Aerodynamics*, **117**, 2013, 38-56